

# The Nature of the New Local Group Dwarf Galaxy Antlia<sup>1</sup>

A. Aparicio<sup>2</sup>

Instituto de Astrofísica de Canarias, E-38200 La Laguna, Tenerife, Canary Islands, Spain.  
e-mail: aaj@iac.es

J. J. Dalcanton<sup>3</sup>

Observatories of the Carnegie Institution of Washington, 813 Santa Barbara St., Pasadena,  
CA 91101, USA. e-mail: jd@ociw.edu

C. Gallart

Observatories of the Carnegie Institution of Washington, 813 Santa Barbara St., Pasadena,  
CA 91101, USA. e-mail: carme@ociw.edu

and

D. Martínez-Delgado

Instituto de Astrofísica de Canarias, E-38200 La Laguna, Tenerife, Canary Islands, Spain.  
e-mail: ddelgado@iac.es

## ABSTRACT

The recently discovered Antlia dwarf galaxy is analyzed using *VI* photometry. The galaxy is resolved into a large number of stars and although the galaxy is intrinsically faint and low surface brightness, its stellar populations reveal characteristics more typical of faint star-forming dIrs rather than dEs. Significant star formation is currently going on in the central part of Antlia although little or no star formation is taking place in the outer regions. This indicates a two-component (core-halo) morphology which appears to be common, not only in large spirals (disk-halo), but in dwarf galaxies as well. The SFR averaged over the lifetime of the galaxy is estimated to be  $\bar{\psi}/A \sim 2 - 4 \times 10^{-10} \text{ M}_{\odot} \text{ yr}^{-1} \text{ pc}^{-2}$  while the more recent star formation, averaged over the last 1 Gyr is much

---

<sup>1</sup>Based on observations made with the 2.5 m Du Pont telescope of the Carnegie Institution of Washington at Las Campanas Observatory in Chile.

<sup>2</sup>Presently at the Observatories of the Carnegie Institution of Washington, 813 Santa Barbara St., Pasadena, CA 91101, USA

<sup>3</sup>Hubble Fellow

higher ( $\bar{\psi}_{1\text{Gyr}}/A \sim 3 - 9 \times 10^{-10} \text{ M}_{\odot}\text{yr}^{-1}\text{pc}^{-2}$  for the central region). The total mass locked into stars and stellar remnants is estimated to be  $M_{\star} \sim 2 - 4 \times 10^6 \text{ M}_{\odot}$ . Its distance, estimated from the TRGB is  $1.32 \pm 0.06 \text{ Mpc}$ , which places Antlia just beyond the Local Group, and makes it a close companion of the dwarf galaxy NGC 3109 ( $\Delta r \gtrsim 30 \text{ kpc}$ ), although it is not clear whether they are gravitationally bound.

## 1. Introduction

Dwarf galaxies are probably the most common type of galaxies in the Universe. At the low end of the mass and luminosity distributions, they span a very wide range of properties and morphologies. Dwarf galaxies can be divided into two large groups: dwarf irregulars (dIrs) and dwarf ellipticals (dEs) (we include in this group the so-called dwarf spheroidal galaxies). In the simplest scheme, the key differences between the two groups are that dIrs have large amounts of gas and high current star formation activity producing many HII regions and blue stars, while dEs lack gas and contain only old ( $> 10 \text{ Gyr}$ ) stars<sup>4</sup>. Morphologically, dIrs tend to be patchy small blue galaxies like NGC 6822 or IC 1613, while dEs show a smooth luminosity distribution (e.g. NGC 147) and in many cases are hardly distinguishable from the sky background, like Sextans or the small Andromeda companions.

However, this picture has been shown to be too simple and the separation between both groups is quite diffuse, if any. On the one hand, there are objects with large amounts of gas but showing an apparently low star formation rate (SFR), such as Pegasus (Aparicio, Gallart, & Bertelli 1997a) or LGS 3 (Aparicio, Gallart, & Bertelli 1997b). These systems have few or no HII regions and lack the patchy morphology of more active dIrs. But, since these galaxies are equally gas rich, the different appearances among dIrs may be the result of episodic star formation, in such a way that some of them are in an active phase of star formation while others are currently quiescent. On the other hand, growing evidence exists that objects traditionally considered to be dEs have a substantial intermediate age stellar population. This was first shown by the discovery of Carbon stars in most of the dE satellites of the Milky Way (see Azzopardi 1994 and references therein) and then beautifully shown in the deep color-magnitude (CM) diagrams obtained for some of these galaxies, like Carina (Smekker-Hane, Stetson, & Hesser 1994), Leo I (Lee et al. 1993a), Fornax (Stetson 1997) and Phoenix (Martínez-Delgado, Aparicio, & Gallart 1998). There is also

---

<sup>4</sup>In this paper, we mean by old stars those older than 10 Gyr, by intermediate-age stars those with ages between 1 and 10 Gyr and by young stars those younger than 1 Gyr.

some evidence of an intermediate age population in the larger dE Andromeda companions, particularly in the cases of NGC 185 (Martínez-Delgado, Aparicio, & Gallart 1997) and NGC 205 (Davidge 1992). Therefore it is not clear where the true dividing line between dIrs and dEs (if any) should be placed; even the gas content, which should tell us about a galaxy’s potential to form stars is not a clear indicator, since galaxies which are apparently devoid of gas, such as Fornax (Stetson 1997), somehow manage to keep forming stars. All this calls to a revision of our current understanding of the nature of dwarf galaxies.

In order to further explore the differences among the dwarf galaxy population, we have undertaken a study of the newly rediscovered Antlia dwarf galaxy. The galaxy had been noted by Crowin et al. (1985); Feitzinger & Galinsky (1985) and Arp & Madore (1987), but was overlooked for a decade. Whiting, Irwin & Haw (1997) rediscovered the galaxy from inspection of the UK Schmidt Telescope plates covering the entire southern sky. Deep CCD images on the 1.5m telescope at Cerro Tololo Observatory performed by these authors revealed it completely resolved into individual stars, indicating that it was probably a new Local Group member. From wide band and  $H_\alpha$  images, these authors observed no hot blue stars nor any obvious trace of star forming regions. They concluded that the galaxy is a typical dE similar to the Milky Way satellites and to the Tucana dwarf. They estimate the distance to be about 1.15 Mpc and its diameter 1–2 Kpc.

We have performed deep  $VI$  photometry of the galaxy resolving a large number of stars. In contrast to Whiting et al. (1997), our results show that star formation is currently taking place (or stopped just a few Myr ago) in the central part of Antlia, making it similar to the smallest, faintest dIr galaxies like Pegasus, LGS 3 or Phoenix. The paper is organized as follows. Section 2 briefly presents the observations. In §3 an overview of the CM diagram is given and used to estimate the distance to Antlia and its metallicity. In §4 the integrated light distribution is discussed. The star formation history (SFH) is sketched in §5, through comparison to other well studied faint dIrs. Finally, the results are summarized in §6.

## 2. Observations, data reduction and photometry

Observations of the Antlia dwarf were made at Las Campanas Observatories on the nights of April 10-12 and April 14, 1997 under photometric conditions, using the Dupont 2.5m telescope with a 2048×2048 thinned Tektronics chip with 0.259"pixels, a gain of 2.2  $e^-$ /adu, and a read noise of 6.6  $e^-$ . The journal of observations is given in Table 1.

All images were bias subtracted using the overscan region, and corrected for residual 2-dimensional structure using a bias frame. Dome flats were used to remove pixel-to-pixel

and large scale variations in the chip response. A fringe frame was created from a median all of the images taken on the night of April 14th of high latitude nearly-blank fields and was subtracted from all  $I$  band images, after matching the sky levels. The sky in the resulting frames is flat to within 0.7%.

Photometry of the stars in Antlia has been performed using the new DAOPHOT/ALLSTAR/ALLFRAME software, made available to us by Dr. Stetson (see Stetson 1994). A master frame has been produced using the best seeing images, both  $V$  and  $I$ , obtained throughout the run. The total integration times are 2400 sec in  $V$  and 2400 sec in  $I$  and the FWHM of the stellar images is  $0.8''$  for the combined image. Three FIND/ALLSTAR/SUBSTAR passes have been used to identify stars in this master frame. The resulting list, consisting on 6831 stars, has been given to ALLFRAME to perform the photometry in the 16 individual frames using quadratically varying PSFs computed for each individual frame. The  $V$  and  $I$  magnitudes for the stars have been obtained as the robust average of the magnitudes obtained in the individual frames. Only stars that have been measured in at least three images have been considered. The resulting  $V$  and  $I$  photometry lists have been paired using DAOMASTER. A final list of 5566 stars is the result of this process. This catalogue of stars has been filtered using the error parameters given by ALLFRAME, retaining only stars with acceptable CHI and SHARP parameters and  $\sigma_V \leq 0.2$  and  $\sigma_I \leq 0.2$ .

Aperture corrections have been obtained using a large number of well measured stars in one  $V$  and one  $I$  image of Antlia. They are accurate to  $\pm 0.005$  mag in  $V$  and  $\pm 0.008$  mag in  $I$ . Extinction for each night and the final transformation to the Johnson-Cousins standard system has been computed using several standards in the list of Landolt (1992) observed repeatedly throughout each of the nights. Color terms have been found to be comparable to the dispersion of the data and have not been used. The standard errors of the extinctions are always smaller than 0.01, while the standard errors in the zero points are  $\pm 0.005$  magnitudes in  $V$  and  $\pm 0.006$  magnitudes in  $I$ . The total errors in the zeropoint of the photometry are therefore about 0.01 in both  $V$  and  $I$ .

Figure 1 shows the  $I$  image of Antlia. For the analysis of the stellar content (see §3 and §5), the observed field has been divided into several parts. Region A corresponds to the central part of Antlia; region B covers the optical external part of the galaxy and regions C map the foreground field stars. A finding chart of the resolved stars with well measured photometry is shown in Fig. 2 (see §3.1). The central part is displayed in Fig. 3, which shows the beautiful resolution into stars of the central part of Antlia. The circle indicates a possible HII region in the center of this region, which corresponds to a large concentration of blue stars. That this central object is actually an HII region needs to be confirmed with

deep  $H_\alpha$  observations.

### 3. The Color-Magnitude Diagram, the Metallicity and the Distance

#### 3.1. The Color-Magnitude Diagram: Subtraction of Foreground Population and Reddening

The CM diagrams of regions A, B and C (see Fig. 1) are shown in Fig. 4. Panels [a] and [b] show the CM diagrams of the inner (A) and outer (B) galaxy. Panels [c] and [d] are CM diagrams of the external (C) regions. They show only a randomly chosen fraction of the stars in these regions such that sampled areas are the same as those of regions A and B, respectively; no attempt has been made to correct for the difference in crowding between the galaxy and field regions. These diagrams have been used to remove foreground stars from diagrams [a] and [b]. To do so, for each star in the foreground frames ([c] & [d]), we select all the stars of the corresponding galaxy frame which lie within a range of magnitude and color around the selected foreground star. This range is the ALLFRAME error corresponding to the magnitude of the foreground star. In a second step, one of the selected stars is randomly chosen and removed. If no stars happen to be inside the error interval, then the nearest one within 0.5 magnitudes is removed. The resulting clean diagrams are plotted in panels [e] and [f]. Field subtraction in the central region (A) is quite independent on the particular subsample of field stars used, due to the low percentage of foreground stars. This is not the case for the low surface brightness outer region (B), and particularly affects the blue stars and those above the TRGB. Thus, it cannot be ruled out that the few stars that remain in these regions in the outer galaxy result from bad field subtraction. Foreground stars as well as those removed from regions A and B are plotted with small dots in Fig. 2. The open circles mark the stars that have been left in the CM diagrams as galaxy members after the field subtraction, and the filled triangles mark blue stars from panels [e] and [f] in Fig. 4.

The Antlia  $[(V - I), I]$  CM diagram shows characteristics typical of the CM diagrams of other dIr galaxies, with evidence for both an old and a young population. The old and intermediate age population clump together in what we are calling the *red-tangle* (see Aparicio, & Gallart 1994), which corresponds to the RGB and AGB locii. The red tangle is the most prominent feature of the Antlia CM diagram, running from  $[(V - I), I] \simeq [1.0, 24.0]$  to  $[1.5, 21.5]$ . There is also a considerable population of blue stars ( $(V - I) \lesssim 0.7$ ) in the CM diagram of the central region (panel [e] of Fig. 4). It is remarkable that these blue stars are entirely absent from the CM diagram of the outer part of the galaxy (panel [f]). The presence of these stars in the central region, as well as the candidate HII region (Fig. 3),

support the idea that Antlia is a dIr galaxy rather than a dE (see §5). Most of the bright stars ( $I \lesssim 21$ ) are likely foreground stars.

The diagrams shown in Fig. 4 have not been corrected for interstellar extinction. However, the extinction must be considered in the forthcoming calculation of metallicity and distance. The galactic coordinates of Antlia are  $l_{\text{II}} = 263^{\circ}.09$ ,  $b_{\text{II}} = 22^{\circ}.32$ , which lies in a region of moderate gradient and between the isolines corresponding to  $E(B - V) = 0.03$  and  $E(B - V) = 0.06$  in the extinction maps of Burstein & Heiles (1982). Neglecting internal reddening, we assume  $E(B - V) = 0.045 \pm 0.015$ . Using the extinction law of Cardelli, Clayton, & Mathis (1989) with  $R_V = 3.3$ , the extinctions in  $V$  and  $I$  are  $A_V = 0.15 \pm 0.05$  and  $A_I = 0.07 \pm 0.03$ .

### 3.2. Metallicity

The average stellar metallicity can be obtained from  $(V - I)_{-3.5}$ , which is the color index of the RGB half a magnitude below the TRGB (see Da Costa & Armandroff 1990; Lee, Freedman, & Madore 1993b). We have estimated  $(V - I)_{-3.5}$  from the median of the stars with colors in the interval  $1.2 < (V - I) \leq 1.8$  and with magnitudes in the interval  $22.04 < I \leq 22.24$  (the magnitude of the TRGB is  $I_{\text{TRGB}} = 21.64$ ; see §3.3). We find  $(V - I)_{-3.5} = 1.45$ , with a color dispersion of  $\pm 0.07$ . Similar values are obtained using stars in the outer region B: 1.46 and 0.08, respectively. The photometric error yielded by ALLFRAME at this magnitude is about  $\pm 0.025$ . As shown by Aparicio & Gallart (1995) and Gallart, Aparicio, & Vílchez (1996a), the actual external errors affecting the photometry cannot be in general estimated from this and are quite dependent on other observational effects (crowding, blending and others). However, the fact that we obtain quite similar values for the color dispersion in central and outer regions indicates that these effects are small and that probably, most of the observational dispersion is due to signal-to-noise at these magnitudes. In these conditions, ALLFRAME errors may be a reasonable estimate of the actual total errors. Furthermore, considering that at the magnitude we are dealing with, the photometric uncertainty is small compared with the color dispersion we measure, it is reasonable to assume that the latter is a good representation of the intrinsic dispersion. We will use it below to estimate the dispersion in metallicity.

The resulting dereddened value for the color index of the RGB is  $(V - I)_{-3.5,0} = 1.37$ . Using the calibration by Lee et al. (1993b), we obtain a metallicity  $[Fe/H] = -1.6 \pm 0.1$ , corresponding to  $Z = 0.0012 \pm 0.0003$  and in good agreement with the estimate by Whiting et al. (1997). The error has been obtained from propagation of the reddening error. Under the assumption that the color dispersion of the red-tangle is only produced by metallicity

dispersion, the latter is  $-1.9 < [Fe/H] < -1.4$ . For comparison, Fornax has a metallicity of  $[Fe/H] = -1.4$  and Phoenix has a metallicity of  $[Fe/H] = -1.9$ .

### 3.3. Distance

The absolute  $I$  magnitude of the tip of the RGB (TRGB) has proven to be a remarkably good estimator of distance (Lee et al. 1993b). The absolute magnitude of the TRGB is slightly dependent on the metallicity, which we have estimated above in §3.2. To obtain the magnitude of the TRGB we have used the luminosity function (LF) of the stars in the color interval  $1.0 < (V - I) \leq 2.0$  drawn from the central galaxy (region A), after correction for foreground contamination (diagram [e] in Fig. 4). We have computed the LF by counting the stars lying inside an interval of  $\pm 0.2$  magnitudes about a central value of  $I$ . The central value has been varied in steps of 0.02 magnitudes to obtain the LF while reducing the dependence of the results upon the particular choice of bin center. Finally, an edge detecting Sobel filter  $[-1, 0, +1]$  has been applied to the LF. This produces a sharp peak at the TRGB corresponding to  $I_{\text{TRGB}} = 21.64 \pm 0.04$ . The error has been obtained from the width of the peak at 1/3 of its height. The same process applied to the foreground stars alone yields a noisy distribution with a dispersion which is 3.5 times smaller than the height of the peak detected for region A. The resulting dereddened value is  $I_{\text{TRGB},0} = 21.57 \pm 0.05$ . The error has been calculated from the quadratic addition of the Sobel filter and extinction errors.

The color index of the TRGB is necessary to calculate the bolometric correction to be used in the  $I_{\text{TRGB}}$ -distance calibration. It has been estimated from the median color index of the stars with  $1.2 < (V - I) \leq 1.8$  and  $21.64 < I \leq 21.84$ . We find  $(V - I)_{\text{TRGB}} = 1.50$  which when corrected for external extinction yields  $(V - I)_{\text{TRGB},0} = 1.42$ .

Using the calibration by Lee et al. (1993b), we obtain a distance modulus  $(m - M)_0 = 25.6 \pm 0.1$ , corresponding to  $1.32 \pm 0.06$  Mpc. The intrinsic error of the method is about  $\pm 0.1$  (see Lee et al. 1993a). This is the adopted error since it is larger than the photometric and extinction ones. Although marginally compatible, our distance is slightly larger than the result by Whiting et al. (1997). The reason for the disagreement might be an upward shift of the TRGB in Whiting et al. CM diagram due to crowding effects at the level of their limiting magnitude.

Antlia lies  $\sim 1.2^\circ$  South from NGC 3109 and both galaxies lie at the same distance, inside the error intervals (see Capaccioli, Piotto & Bresolin 1992; Lee 1993; Davidge 1993). Assuming the same distance for both galaxies, their minimum physical separation is  $r = 29$

Kpc. However, if the distance of NGC 3109 is assumed to be  $1.26 \pm 0.1$  Mpc (Capaccioli et al. 1992; Lee 1993), and the errors are considered, the true separation could be as large as 180 Kpc. In spite of their close proximity, the difference in the velocities makes not clear whether Antlia is gravitationally bound to NGC 3109. Assuming a mass of  $8.6 \times 10^9 M_\odot$  for NGC 3109 (Jobin & Carignan 1990), and circular orbits, Antlia would be unbound if the relative velocity exceeded only  $51 \text{ km/s} \times (r/29\text{Kpc})^{-1/2}$ . The radial velocity of NGC 3109 is  $406 \text{ Kms}^{-1}$  (Hartmann 1994 and 1997), while that of Antlia is  $361 \text{ Kms}^{-1}$  (Fouqué et al. 1990). This means that the galaxies would be unbound if the relative distance is  $r \gtrsim 37$  Kpc. Considering that still smaller values will be in general expected for non-circular orbits, it is more likely that either they are both bound to the larger mass of the Local Group (although van den Bergh 1994 places NGC 3109 just beyond the gravitational limit of the Local Group), or they are members of a common filament feeding into the Local Group region.

#### 4. Integrated Light

To determine the total magnitude, color, and surface brightness distribution of Antlia, we have fit its surface brightness distribution with ellipses of ellipticity  $e = 1 - b/a = 0.4$  and semi-major axis at position angle  $135^\circ$  (measured from North to East), in both the  $V$  and the  $I$  bands, after masking out stars which were too bright to be members of the galaxy (e.g.  $I < 21$ ). The sky was subtracted using the median surface brightness distribution in the ellipses beyond a radius of  $2'$ .

The resulting  $V$ -band surface brightness distribution is shown in Figure 5 as a function of the ellipse semi-major axis  $a$ . In both the  $V$  and  $I$  bands, the surface brightness distribution is fairly flat to a radius of  $\sim 40''$ , which corresponds roughly to the extent of the central galaxy defined by region (A), and then falls off more steeply at larger radii. This is comparable to the profiles of the faint Andromeda companions And I, And II, & And III, reported by Caldwell et al. (1992). The  $V$  band surface brightness can be well fit by a double exponential profile with central surface brightness  $\mu_0(V) = 24.3 \text{ mag}/(")^2$  and exponential scale length  $\alpha = 64''$  in the inner regions ( $a < 40''$ ), and  $\mu_0(V) = 22.4 \text{ mag}/(")^2$  and  $\alpha = 16.5''$  at larger radii. This gives an angular diameter at the  $\mu_V = 26 \text{ mag}/(")^2$  isophote of  $\theta_{26} = 1.8'$ ; this corresponds to an isophote of  $\mu_I = 25.1 \text{ mag}/(")^2$ . Given the distance of the galaxy, the break in the surface brightness profile occurs at  $a = 0.26$  Kpc, and the inner and outer scale lengths are 0.36 Kpc and 0.14 Kpc, respectively.

Integrating the surface brightness profiles within the  $V$  and  $I$  bands out to the  $\mu_V = 26 \text{ mag}/(")^2$  isophote, we find  $m_V = 15.67 \pm 0.12$ , and  $m_I = 14.91 \pm 0.12$ , uncorrected



for internal or galactic extinction. The quoted errors are an upper limit computed assuming that every point in Fig. 5 were systematically off by  $1 \sigma$ . Following de Vaucouleurs et al. (1991), the internal extinction of Antlia can be estimated to be  $A_{B,i} = 0.30$ . Using the extinction law by Cardelli et al. (1989) with  $R_V = 3.3$  this yields  $A_{V,i} = 0.23$  and  $A_{I,i} = 0.11$ . After correction for internal and external extinction and considering the error in the distance modulus, the total absolute magnitude of Antlia is  $M_{V,0} = -10.3 \pm 0.2$  and  $M_{I,0} = -10.9 \pm 0.2$ . The luminosity of Antlia is therefore comparable to the faintest dIrs, making Antlia an extremely faint galaxy in spite of its recent star formation. The mean color of Antlia is quite blue:  $(V - I)_0 = 0.6 \pm 0.2$ , and is comparable to the colors of galaxy types Scd & Im ( $(V - I) = 0.82$ ) for the Coleman et al. (1980) composite spectral energy distributions, and Im ( $(V - I) = 0.64$ ) for the SEDs reported by Fukugita et al. (1995).

## 5. Clues to the Star Formation History

The color magnitude diagrams presented in §3 clearly show that Antlia has had an extended star formation history, as evidenced by its old and intermediate age red-tangle and its population of young, blue stars. We can sketch the SFH of Antlia in more detail by comparing Antlia with two faint, low surface brightness dIrs whose CM diagrams are similar to Antlia’s and whose star formation histories have been well studied: Pegasus (Aparicio et al. 1997a) and LGS 3 (Aparicio et al. 1997b). The SFHs of these galaxies have been determined from their resolved stellar content (former references), hence from information similar to the one available for Antlia. It turns out, as we will see below, that Antlia has characteristics intermediate between these two galaxies.

Figure 6 shows the CM diagrams of the central and outer regions of Antlia compared with those of Pegasus and LGS 3. An isochrone from the library of Padua (see Bertelli et al. 1994) of 0.1 Gyr and  $Z = 0.001$  for Antlia and LGS 3 and the same age and  $Z = 0.004$  for Pegasus, is overplotted in the four diagrams. The isochrone qualitatively shows that the blue stars present in the CM diagrams of the central region of Antlia are likely young main-sequence (MS) and/or blue-loops (BL) stars a few hundred Myr old, indicating that recent star formation activity has taken place in the central part of the galaxy. The few stars observed above the TRGB (within  $\sim 1$  magnitude) in Antlia’s central CM diagram are likely intermediate-age AGB stars, similar to what are observed in Pegasus and, to a lesser extent, in LGS 3. These stars indicate star formation activity at intermediate ages. A few of these blue stars and likely intermediate age stars are also seen in the outer regions of Antlia, but, as stated above, they may also result from incomplete field subtraction in the more highly contaminated outer regions. The fact that Antlia lacks an extended AGB

red tail structure like Pegasus (seen redward of  $(V - I) = 2$ , at  $M_I = -3.5$ ), is consistent with its low metallicity (Aparicio & Gallart 1994).

If star formation has been very recent in the central region, HII regions would be expected. However, conspicuous HII regions are not necessarily required if the star formation is going on at a slow rate. This is also the case of both Pegasus and LGS 3. Interestingly, a feature is seen in our images of Antlia that could be a small HII region. It is marked with a circle in Fig. 3 and its position corresponds to the clump of blue stars at  $(x, y) \simeq (700, 950)$  shown in Fig. 2. If the feature proves to be an HII region, it would be definitive evidence of significant star formation activity in the last  $\sim 10$  Myr.

The SFHs of Pegasus (Aparicio et al. 1997a) and LGS 3 (Aparicio et al. 1997b) have been obtained from comparison of their CM diagrams with a large set of model CM diagrams computed for different SFRs and chemical enrichment laws. We will compare the CM diagram of Pegasus and LGS 3 with that of Antlia to provide an insight to its SFH. Gallart et al. (1996b) showed that the distributions of stars older and younger than  $\sim 1$  Gyr are decoupled in a CM diagram like that of Antlia: almost no stars older than 1 Gyr are among the blue population and almost no stars younger than that age populate the red-tangle region. On the other hand, the amount of blue and red-tangle stars should be related to the SFR  $\psi(t)$ , integrated over the appropriate time intervals. Therefore the number of blue and red stars in Antlia, compared to that in Pegasus and LGS 3, will constrain Antlia’s SFH. The results are summarized in Table 2 where the number of red and blue stars, the ratio between them and the SFR averaged for the whole life of the galaxies ( $\bar{\psi}$ ) and for the last 1 Gyr ( $\bar{\psi}_{1\text{Gyr}}$ ) are given. The SFR values for Antlia are given in brackets, indicating that they are estimates from comparison with the other two galaxies, derived by scaling the SFR in LGS 3 and Pegasus to the relative number of blue and red stars. Data for the inner (A) and outer (B) regions of Antlia are considered separately. Only the stars between the TRGB and 1.5 magnitudes in  $I$  below it have been considered. To separate the stars into blue and red categories, the median  $(V - I)$  of the RGB at  $I = I_{\text{TRGB}} + 1.5$  has been used as reference. The stars are counted as blue when they are at least 0.5 magnitudes bluer than that  $(V - I)$ ; otherwise, they are counted as red.

The numbers of red and blue stars listed in Table 2 suggest that both the recent and the past SFR in the central part of Antlia, have been intermediate between those of LGS 3 and Pegasus. In the center of Antlia, the galaxy has been forming stars for the last 1 Gyr at roughly twice its normal rate, whereas in Pegasus, the recent star formation is comparable to the average lifetime SFR, and in LGS3, the recent SFR is a factor of three smaller than its lifetime average. In the outer regions of Antlia, it seems that the past SFR was much higher than it has been in the most recent 1 Gyr. However, the small upper limit given for

the current SFR in the outer region is highly uncertain because of the uncertainties of the foreground stars subtraction in the more heavily contaminated outer galaxy region.

Table 3 summarizes the SFR normalized by the galaxies’ area and some integrated physical parameters for Antlia, Pegasus, and LGS 3. The areas of Antlia regions A and B are  $3.06 (')^2$  and  $11.29 (')^2$  respectively, which correspond to  $4.51 \times 10^5 \text{ pc}^2$  and  $1.66 \times 10^6 \text{ pc}^2$ , respectively. The values for Pegasus (see Aparicio et al. 1997a and references therein) and LGS 3 (see Aparicio et al. 1997b and references therein) are also given for comparison. The distance of Antlia from the barycenter of the Local Group has been calculated assuming the latter is 0.45 Mpc from the Milky Way towards Andromeda (see Aparicio et al. 1997b and references therein). To calculate  $M_{V,0}$ , the integrated  $V_T$  magnitude of Pegasus and LGS 3 given respectively by de Vaucouleurs et al. (1991) and by Karachentseva et al. (1997) have been used. The absolute magnitude of the Sun has been assumed to be  $M_{V\odot} = 4.87$  (Durrant 1981). The total mass in stars and stellar remnants ( $M_*$ ) of Antlia has been calculated from  $\bar{\psi}$  and  $\bar{\psi}_{1\text{Gyr}}$  for the central and outer regions. The value of the gas mass ( $M_{\text{gas}}$ ) has been calculated using the data by Fouqué et al. (1990); the relationship given by Hoffman et al. (1996) for the HI mass, and assuming that  $M_{\text{gas}} = 4/3 M_{\text{HI}}$ . The total mass ( $M_{\text{tot}}$ ) has been estimated using the relation  $M_{\text{tot}} = 9.3 \times 10^5 \bar{r}_H \sigma^2$  given by Lo, Sargent, & Young (1993), which assumes virial equilibrium.  $\bar{r}_H$  has been obtained as  $(a \times b)^{1/2}$ , where  $a = 0.7 \text{ Kpc}$  is the semimajor axis of the galaxy at the  $\mu_V = 26 \text{ mag}/(')^2$  isophote;  $b = 0.4$  is the semiminor axis, calculated using the ellipticity  $e = 0.4$  (see sec. 4) and  $\sigma = 9 \text{ Km s}^{-1}$  is the velocity dispersion estimated from the value of  $W_{50}$  given by Fouqué et al. (1990), assuming a gaussian profile of the 21 cm line.

The significant recent star formation observed in the central region of Antlia contrasts with the absence of a significant young population in the outer region and may suggest a two components (core-halo or disk-halo) composition of the galaxy. This seems to be common not only in large spirals but also in dwarfs (see for example the case of WLM; Minniti & Zijlstra 1996) indicating that the gas currently participating in the star formation is concentrated in the central part of the galaxy and that the physical mechanisms of galaxy formation are shared by systems in a large range of initial masses. Nevertheless at the distances of the dIr galaxies, it is difficult to ascertain whether what we are observing as a ”halo” consists of a purely ”old” (age  $> 10 \text{ Gyr}$ ) population, or that at the low densities in the outer regions, star formation proceeds much more slowly than in the dense center, such that the quantity of young stars at any time is much smaller than in the central region, and hence virtually unobservable. Note that the structure of the red-tangle in both the central and the outer region is very similar, suggesting similar SFH from 1 Gyr to 15 Gyr for both parts of the galaxy. Although appealing, we argue that this hypothetical, truly dual, core-halo structure in dIr galaxies should be further investigated. The analysis of the

stellar population in a large enough area containing both kind of (core-halo) population, through comparison with model CM diagrams (see Aparicio et al. 1997a and 1997b and Gallart et al. 1997b) may cast some light to this issue.

## 6. Conclusions

We have presented photometry of resolved stars in the recently discovered Antlia dwarf galaxy. Although it is an intrinsically faint, low surface brightness galaxy, Antlia has characteristics of dIr galaxies rather than dEs, at least from the point of view of the relatively large amount of recent star formation detected in its central region. Its HI mass is also compatible with a dIr galaxy. Future measures of its HI and HII contents will help towards understanding its properties.

The stellar component of the galaxy has an average metallicity  $[Fe/H] = -1.6 \pm 0.1$ , corresponding to  $Z = 0.0012 \pm 0.0003$ , similar to the less enriched dIrs and dEs. This places Antlia nicely on the relationships  $[Fe/H] - M_V$  and  $[Fe/H] - \mu_V$  shown by Caldwell et al. (1992). Antlia is at a distance of  $1.32 \pm 0.06$  Mpc, at what is considered to be the outskirts of the Local Group. It is also a close companion ( $29 \text{ kpc} \leq r \leq 180 \text{ kpc}$ ) of NGC 3109, although their relative velocity ( $45 \text{ Kms}^{-1}$ ) makes it unlikely that they form a gravitationally bound pair. They would be bound only if their relative distance is smaller than 37 Kp and the orbit is circular.

Antlia has a light distribution which is well described by a double exponential, with a relatively flat distribution within  $r = 40'$  which steepens at larger radii. Its central surface brightness is  $\mu_0(V) = 24.3 \text{ mag}/('')^2$ , and its isophotal diameter along the semi-major axis is  $\theta_{26} = 1.8'$  or  $D_{26} = 0.7 \text{ kpc}$ , making it an intrinsically small low surface brightness galaxy. Antlia's integrated absolute magnitude within  $\mu_V = 26 \text{ mag}/('')^2$  is  $M_{V,0} = -10.3 \pm 0.2$ , making it among the lowest luminosity galaxies known. It is also quite blue ( $(V - I) = 0.6 \pm 0.2$ ), and is comparable in color to very late type Scd/Im galaxies.

The Antlia SFH has been discussed through comparison with the CM diagrams of Pegasus and LGS 3. Star formation is currently going on (or has stoped within the last few Myr) in the central  $\sim 0.25 \text{ Kpc}$  of Antlia, at a rate at least twice as large as the average for the entire galaxy lifetime (see Table 2). This rate is similar to and probably intermediate between that of Pegasus and LGS 3. Little or no star formation is currently taking place in the outer region of the galaxy. This behaviour seems to be quite common in dwarf galaxies and might be indicative of a core-halo structure in which the gas participating in the star formation would be concentrated towards the center of the galaxy. Nevertheless, we argue

that the question of whether the outer part of the galaxy showing little or no current star formation is or not a *true* halo, composed solely by an old ( $> 10$  Gyr old) population should be further investigated. Given the integrated star formation history, we estimate that the total mass into stars and stellar remnants is  $M_{\star} \sim 2 - 4 \times 10^6 M_{\odot}$ .

We are grateful to Dr. A. Whiting and Dr. M. Irwin for giving us information about the galaxy and for making available to us a preprint of their Antlia paper, and to Dr. W. Freedman for advising us of the previous discovery of the Antlia galaxy by Arp & Madore. We also thank Dr. D. Hartmann for providing us with HI maps of the Antlia/NGC3109 region. AA thanks the Observatories of the Carnegie Institution for its hospitality. AA is financially supported by the Instituto de Astrofísica de Canarias (grant P3/94) and by the Dirección General de Enseñanza Superior of the Kingdom of Spain (grant PB94-0433). Support for JJD was provided by NASA through Hubble Fellowship grant #2-6649 awarded by the Space Telescope Science Institute, which is operated by the Association of Universities for Research in Astronomy, Inc., for NASA under contract NAS 5-26555. DMD is financially supported by the Instituto de Astrofísica de Canarias (grant P3/94).

## REFERENCES

- Aparicio, A., & Gallart, C. 1994, in *The Local Group: comparative and global properties*, ESO Conference and Workshop Proceedings No. 51, ed. A. Layden, R. C. Smith, & J. Storm (Garching: ESO), 115
- Aparicio, A., & Gallart, C. 1995, *AJ*, 110, 2105
- Aparicio, A., Gallart, C., & Bertelli, G. 1997a, *AJ*, in press
- Aparicio, A., Gallart, C., & Bertelli, G. 1997b, *AJ*, in press
- Arp, H.C. & Madore, B.F. 1987, "A catalogue of southern peculiar galaxies and associations. Vol. 1: Positions and descriptions" pag. 113, Cambridge University Press
- Azzopardi, M. 1994, in *The Local Group: comparative and global properties*, ESO Conference and Workshop Proceedings No. 51, ed. A. Layden, R. C. Smith, & J. Storm (Garching: ESO), 129
- Arp, H.C. & Madore, B.F. 1987, "A catalogue of southern peculiar galaxies and associations. Vol. 1: Positions and descriptions" pag. 113, Cambridge University Press
- Bertelli, G., Bressan, A., Chiosi, C., Fagotto, F., & Nasi, E. 1994, *A&AS*, 106, 271
- Burstein, D., & Heiles, C. 1982, *AJ*, 87, 1165

- Caldwell, N., Armandroff, T. E., Seitzer, P., & Da Costa, G. S. 1992, *AJ*, 103, 840
- Capaccioli, M., Piotto, G., & Bresolin, F. 1992, *AJ*, 105, 1779
- Cardelli, J. A., Clayton, G. C., & Mathis, J.S. 1989, *ApJ*, 345, 245
- Coleman, C. D., Wu, C.-C., & Weedman, D. W. 1980, *ApJS*43, 393
- Corwin, H. G. jr., de Vaucoulers, A., & de Vaucoulers, G. 1985, *Southern Galaxy Catalog*, University of Texas Monographs #4
- Davidge, T. J. 1992, *ApJ*, 397, 457
- Davidge, T. J. 1993, *AJ*, 105, 1392
- Da Costa, G. S., & Armandroff, T. E. 1990, *AJ*, 100, 162
- de Vaucouleurs, G., de Vaucouleurs, A., Corwin, H.G., Buta, R.J., Paturel, G., & Fouqué, P. 1991, *Third reference Catalog of Bright Galaxies* (New York: Springer-Verlag)
- Durrant, C. J. 1981, *Landolt-Börnstein New Series*, ed. by K.-H. Hellwege, Group VI, ed. K. Schaifers, & H. H. Voigt, vol. 2a, (Berlin-Heidelberg: Springer), 82
- Feitzinger, J. V., & Galinski, Th. 1985, *A&AS*, 61, 503
- Fouqué, P, Bottinelli, L., Durrand, N., Gouguenheim, L, & Paturel, G. 1990, *A&AS*, 86, 473
- Fukugita, M., Shimasaku, K., & Ichikawa, T. 1995, *PASP*107, 945
- Gallart, C., Aparicio, A., Vilchez, J. M. 1996a, *AJ*, 112, 1928
- Gallart, C., Aparicio, A., Bertelli, G., Chiosi, C. 1996b, *AJ*, 112, 1950
- Hartmann, D. 1994, "The Leiden/Dwingeloo Survey of Galactic Neutral Hydrogen", Ph.D. Thesis, University of Leiden
- Hartmann, D. 1997, "Atlas of Galactic Neutral Hydrogen", Cambridge University Press
- Hoffman, G. L., Salpeter, E. E., Farhat, B., Roos, T., Williams, H., & Helou, G. 1996, *ApJS*, 105, 269
- Jobin, M. & Carignan, C. 1990, *AJ*, 100, 648
- Karachentseva, V. E., Prugniel, Ph., Vennink, J., Richter, G., Thuan, T., & Martin, J. 1997, *A&A*, in press
- Landolt, A. U. 1992, *AJ*, 104, 340
- Lee, M. G., Freedman, W. L., Mateo, M., Thompson, I., & Ruiz, M. T. 1993a, *AJ*, 106, 1420
- Lee, M. G., Freedman, W. L., Madore, B. F. 1993b, *ApJ*, 417, 553

Lee, M. G. 1993, ApJ, 408, 409

Martínez-Delgado, D., Aparicio, A., & Gallart, C. 1997, in preparation

Martínez-Delgado, D., Aparicio, A., & Gallart, C. 1998, in preparation

Minniti, D., & Zijlstra, A. A. 1996, ApJ, 463, L13

Smecker-Hane, T. A., Stetson, P. B., & Hesser, J. E. 1994, AJ, 108, 507

Stetson, P. B. 1994, PASP, 106, 250

Stetson, P. B. 1997, Baltic Astronomy, 6, 3

van den Bergh, S. 1994, AJ, 107, 1328

Whiting, A., Irwin, M &, Hau, G. 1997, AJ(in press)

Table 1. Journal of Observations

Date	Time(UT)	Filter	Exp. time (s)	FWHM (")
97.04.12	00:03	V	600	1.15
97.04.12	00:16	V	600	1.12
97.04.12	00:28	V	600	1.14
97.04.12	23:45	I	600	0.75
97.04.13	00:04	I	300	0.67
97.04.13	00:11	I	300	0.75
97.04.13	00:18	I	300	0.72
97.04.13	00:25	I	300	0.70
97.04.13	00:32	I	300	0.78
97.04.13	00:38	I	300	0.75
97.04.13	00:46	V	300	0.98
97.04.13	00:52	V	300	1.00
97.04.13	00:59	V	300	0.90
97.04.14	01:37	V	600	0.96
97.04.14	01:49	V	600	0.85
97.04.14	02:01	V	600	0.83



Table 2. Comparative features and global properties of Antlia

	LGS 3	Pegasus	Antlia (center)	Antlia (outer)
$N_{\text{red}}$	104	1144	299	181
$N_{\text{blue}}$	5	80	49	8
$N_{\text{blue}}/N_{\text{red}}$	0.05	0.07	0.16	0.04
$\bar{\psi}$ ( $M_{\odot}\text{yr}^{-1}$ )	$4 \times 10^{-5}$	$6.7 \times 10^{-4}$	$[1 - 2 \times 10^{-4}]$	$[0.5 - 1 \times 10^{-4}]$
$\bar{\psi}_{1\text{Gyr}}$ ( $M_{\odot}\text{yr}^{-1}$ )	$1.5 \times 10^{-5}$	$6.2 \times 10^{-4}$	$[1.5 - 4 \times 10^{-4}]$	$[< 3 \times 10^{-5}]$

Table 3. Comparative features and global properties of Antlia

	Antlia (center)	Antlia (outer)	LGS 3	Pegasus
$\bar{\psi}/A$ ( $M_{\odot}\text{yr}^{-1}\text{pc}^{-2}$ )	$2 - 4 \times 10^{-10}$	$3 - 5 \times 10^{-11}$	$1.4 \times 10^{-10}$	$1.5 \times 10^{-9}$
$\bar{\psi}_{1\text{Gyr}}/A$ ( $M_{\odot}\text{yr}^{-1}\text{pc}^{-2}$ )	$3 - 9 \times 10^{-10}$	$< 10^{-11}$	$5.5 \times 10^{-11}$	$1.4 \times 10^{-9}$
$Z$		0.0012	0.0014	0.002
Distance (Mpc)		1.32	0.77	0.95
Distance to LG (Mpc)		1.72	0.37	0.64
$M_{V,0}$		-10.3	-9.28	-12.55
$L_V$ ( $L_{\odot}$ )		$1.2 \times 10^6$	$4.5 \times 10^5$	$9.3 \times 10^6$
$M_{\star}$ ( $M_{\odot}$ )		$2 - 4 \times 10^6$	$4.8 \times 10^5$	$10^7$
$M_{\text{gas}}$ ( $M_{\odot}$ )		$(1.1 \pm 0.2) \times 10^6$	$3.2 \times 10^5$	$6.5 \times 10^6$
$M_{\text{tot}}$ ( $M_{\odot}$ )		$(4.1 \pm 0.8) \times 10^7$	$1.8 \times 10^7$	$1.8 \times 10^8$

Fig. 1.— *I* image of Antlia. The total field is  $7.8' \times 6.9'$  and the integration time 2400 s. The central (A) and outer (B) regions in which the galaxy has been divided for its study are shown. The two regions marked (C) have been used for foreground subtraction. North is up, east is left. **Note:** this figure is sent separately in gif format to reduce size

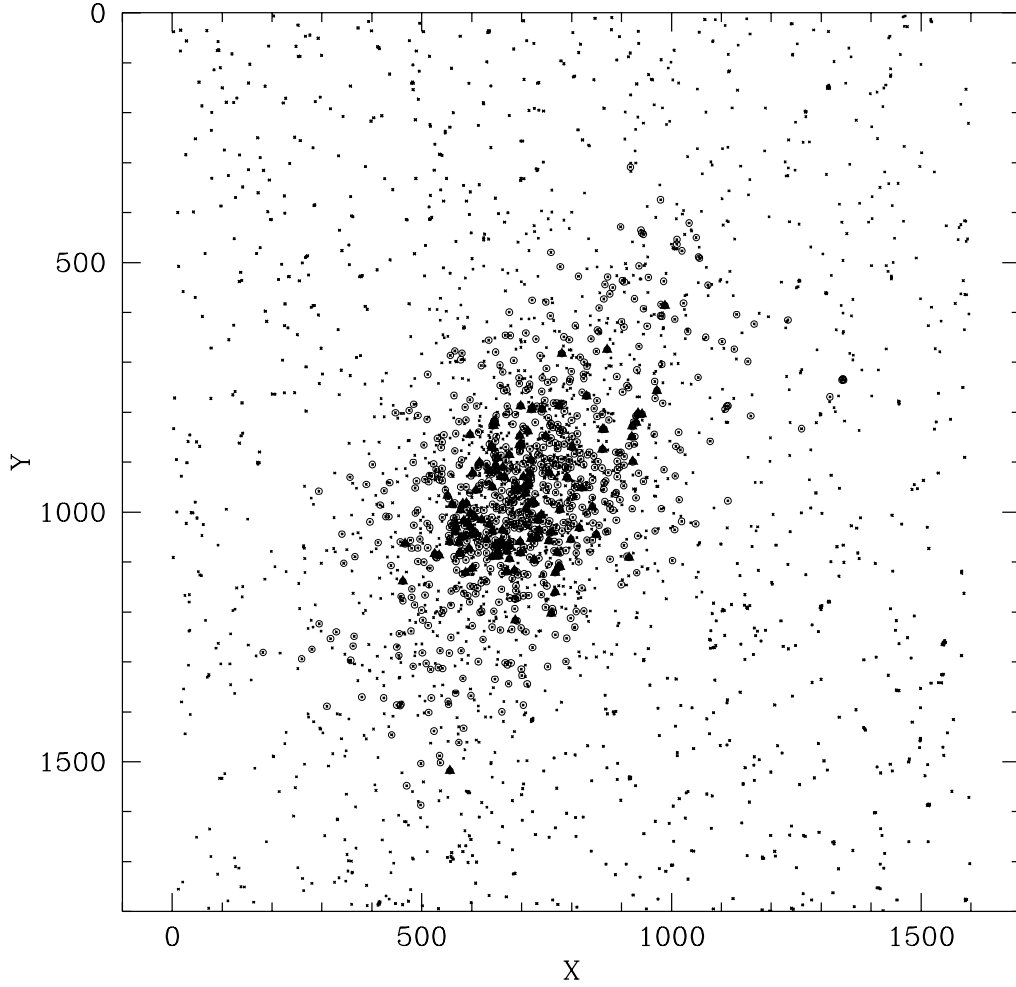


Fig. 2.— Finding chart of the resolved stars. Large filled triangles represent Antlia stars bluer than the diagonal lines in Fig. 4. Open circles are Antlia stars redward of these lines. Small dots represent foreground stars. The plain small dots inside regions A and B represent the stars that have been eliminated from the CM diagrams of these regions in the field subtraction process. The axes are given in pixels ( $0.259''/\text{pixel}$ ).

Fig. 3.— *I* image of the central part of Antlia. The total field is  $2.2' \times 2.2'$  and the integration time 2400 s. The circle shows a possible HII region. North is up, east is left. **Note:** this figure is sent separately in gif format to reduce size

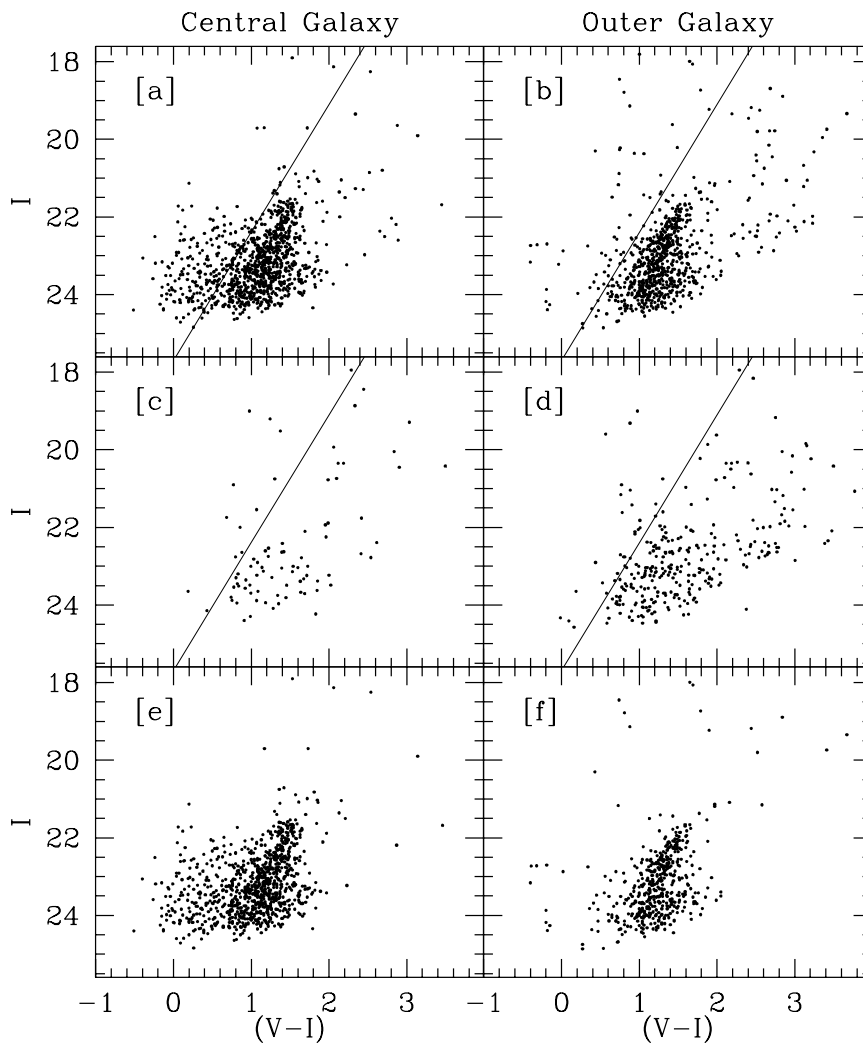


Fig. 4.—  $I$  vs.  $(V - I)$  CM diagrams for different regions of the observed field. [a] Antlia central region (A of Fig. 1); [b] Antlia outer region (B of Fig. 2); [c] and [d] external foreground regions (C of Fig. 1) normalized to the areas covered in panels [a] and [b] respectively; [e] and [f], the same diagrams shown in panels [a] and [b] after subtraction of foreground stars. Diagonal lines show the line used to discriminate blue and red stars in Fig. 2.

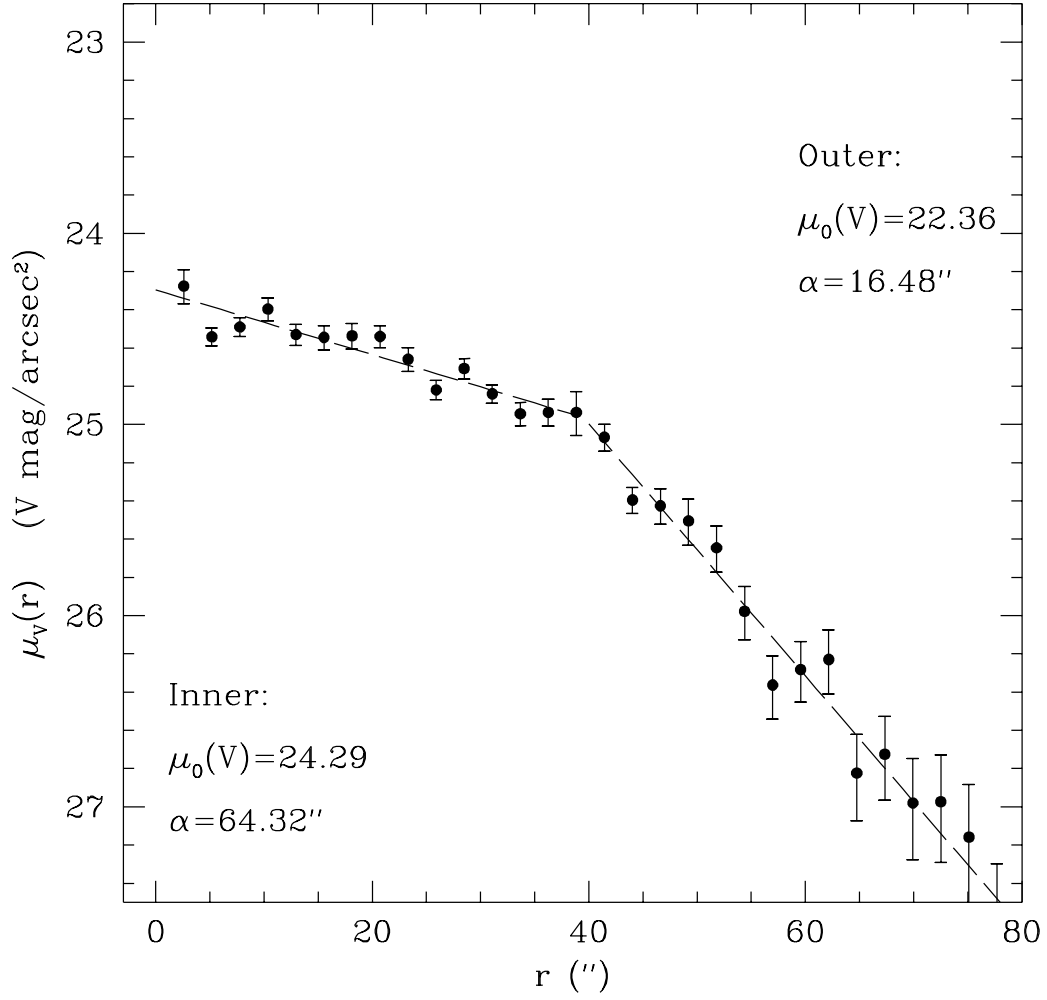


Fig. 5.—  $V$  surface brightness distribution as a function of semimajor axis. It can be fitted by two exponential laws with the indicated parameters. The  $1\sigma$  error bars are calculated as the quadrature sum of the uncertainties in the mean number of counts in a given annulus and the uncertainty in the sky subtraction.

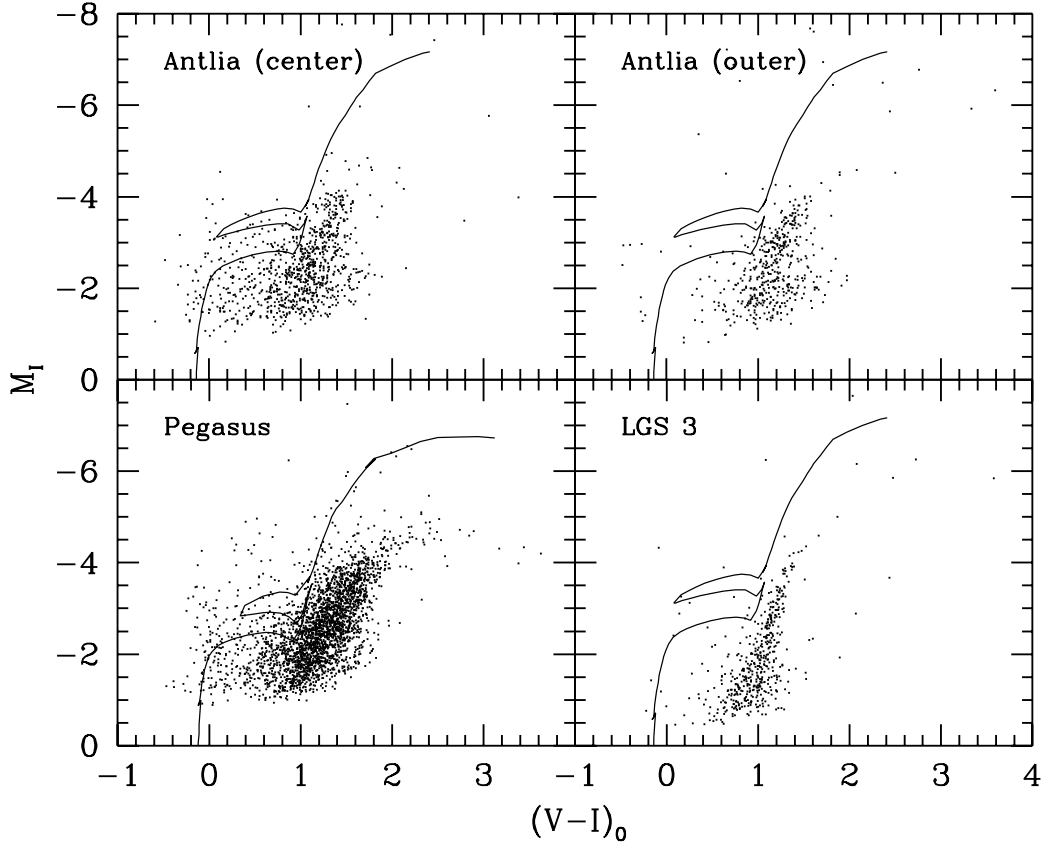


Fig. 6.—  $M_{I,0}$  vs.  $(V-I)_0$  CM diagrams of the central and outer regions of Antlia compared to those of Pegasus and LGS 3. An isochrone from the library of Padua (see Bertelli et al. 1994) of 0.1 Gyr and  $Z = 0.001$  for Antlia and LGS and the same age and  $Z = 0.004$  for Pegasus is overplotted.

This figure "antlia.fig1.gif" is available in "gif" format from:

<http://arxiv.org/ps/astro-ph/9706197v1>



This figure "antlia.fig3.gif" is available in "gif" format from:

<http://arxiv.org/ps/astro-ph/9706197v1>